

Indian summer monsoon forcing on the deglacialpolar cold reversals

Virupaxa K. Banakar*^{1,2}, Sweta Baidya^{1,2}, Alexander M. Piotrowski³, D. Shankar¹

¹CSIR-National Institute of Oceanography, Dona Paula, Goa 403004, India

²Academy of Scientific and Innovative Research (AcSIR), CSIR-NIO, Goa, India

³Department of Earth Sciences, University of Cambridge, CB2 3EQ, Cambridge, UK

*Correspondence to: virupaxa56@gmail.com

Abstract

The deglacial transition from the last glacial maximum at ~20 kiloyears before present (ka) to the Holocene (11.7 ka to Present) was interrupted by millennial-scale cold reversals viz., Antarctic Cold Reversal (~14.5-12.8 ka) and Greenland Younger Dryas (~12.8 -11.8 ka) which had different timings and extent of cooling in each hemisphere. The cause of this synchronously initiated, but different hemispheric cooling during these cold reversals (Antarctic Cold Reversal ~3°C and Younger Dryas ~10°C) is elusive because CO₂, the fundamental forcing for deglaciation, and Atlantic meridional overturning circulation, the driver of antiphased bipolar climate response, both fail to explain this asymmetry. We use centennial-resolution records of the local surface water $\delta^{18}\text{O}$ of the Eastern Arabian Sea, which constitutes a proxy for the precipitation associated with the Indian Summer Monsoon, and other tropical precipitation records to deduce the role of tropical forcing in the polar cold reversals. We hypothesize a mechanism for tropical forcing, via the Indian Summer Monsoons, of the polar cold reversals by migration of the Inter-Tropical Convergence Zone and the associated cross-equatorial heat transport.

Introduction

Palaeo records show that during the last deglaciation, polar regions warmed and cooled asymmetrically, with more gradual and less extreme changes in the south (Blunier and Brook 2001; Shakun *et al.* 2012). The initial deglacial warming of $\sim 6^{\circ}\text{C}$ ($\sim 18\text{-}14.5$ ka) in Antarctica was gradual (Parrenin *et al.* 2007), but the Greenland warmed rapidly by $\sim 11^{\circ}\text{C}$ (≈ 7 ‰ increase of $\delta^{18}\text{O}_{\text{ICE}}$) during Bølling (15-14.4 ka) (Jouzelet *et al.* 1995; Johnsen *et al.* 1992). During the following ~ 0.5 ky, the Antarctic cooled by $\sim 3^{\circ}\text{C}$, but this cooling paused for ~ 1.5 ky to form the Antarctic Cold Reversal (ACR: $\sim 14.5\text{-}12.8$ ka). The ACR overlapped the $\sim 5^{\circ}\text{C}$ cooling (~ 3 ‰ decrease of $\delta^{18}\text{O}_{\text{ICE}}$) during post-Bølling that formed the Ållerød ($\sim 14.5\text{-}12.8$ ka); subsequently, Greenland cooled by a further $\sim 5^{\circ}\text{C}$ to form the coldest Younger Dryas (YD: 12.8–11.8 ka). Thus, the Ållerød and YD together form the Greenland cold reversal (14.5 – 11.8 ka), similar to the ACR in Antarctic. Considering the polar temperatures at the end of Last Glacial Maximum (LGM) as reference temperatures for the respective hemispheres, the subsequent deglacial bipolar thermal contrasts are distinctly different during cold reversals.

The role of CO_2 in causing these deglacial cold reversals can be ruled out because a corresponding depletion in its atmospheric concentration did not occur during these cold reversals: instead, CO_2 concentration remained constant at ~ 240 ppmv (Monnin *et al.* 2001). An anti-phased inter-hemispheric ocean-heat-budget is a necessity for the operation of Atlantic Meridional Overturning Circulation (AMOC: Barker *et al.* 2009; Clement and Peterson 2008; Crowley 1992; Wunch 2006). Therefore, the AMOC is an unlikely driver of observed polar cold reversals because the cooling is synchronous in both Antarctic and Greenland ice-core records during ACR-Ållerød. Further, the YD fingerprint is not observed in subtropical sea surface temperature (SST) time series of the southern hemisphere (Calvo *et al.* 2007).

Tropical climate has generally been considered to respond to the rapid changes in Greenland, with the AMOC providing the teleconnection (Deplazes *et al.* 2013; Hong *et al.* 2003; Kessarkar *et al.* 2013; Marzin *et al.* 2013; Mohtadi *et al.* 2014), but dry and windy events in tropical East Africa preceding the Greenland stadials argue against this teleconnection (Brown *et al.* 2007). Such discrepancies with the AMOC hypothesis have led researchers to consider the tropics also as a possible forcing (Cane 1998; Koutavas *et al.* 2002; Wunch 2006). However, formal mechanisms to link tropical forcing on extratropical climate change in the past are still in the formative stage (Chiang 2009). In this paper, we present a mechanism that links changes in the tropics (specifically the monsoon regime) to synchronous but differential cooling during the polar cold reversals. This mechanism invokes the migration of the Inter-tropical Convergence Zone (ITCZ) and associated

changes in monsoon precipitation, which together form a major cross-equatorial heat engine, and can be tested by reconstructing the sequence of deglacial changes in the tropics relative to the poles.

The seasonal latitudinal migration of the ITCZ is limited to $\sim 7^\circ$ over most of the Pacific except the western Pacific warm pool and the Atlantic (Philander *et al.* 1996; Schneider *et al.* 2014). The latitudinal displacement of the Pacific and Atlantic mean ITCZ position in the past is also limited to $\sim 0.6^\circ$ (McGee *et al.* 2014). In contrast, the ITCZ position swings by $\sim 28^\circ$ seasonally over the Indian Ocean and over the western Pacific warm pool (Fig. 1), which is warmer and transfers this heat to the atmosphere (Waliser and Jiang 2014). The ITCZ extends farther into the northern hemisphere (to the foothills of the Himalayas) than elsewhere owing to the South Asian summer monsoons (Gadgil 2003). The monsoon is associated with latent-heat release in the mid-troposphere and this heat is transported southward across the equator via the descending limb of the southern Hadley Cell (Heaviside and Czaja 2013). Studies show that the moisture-laden, low-level Somali Jet (Findlater 1969) that feeds the ISM contributes more thermal energy to the cross-equatorial heat budget than do the Pacific and Atlantic ITCZs (Heaviside and Czaja 2013).

At present, the net global cross-equatorial atmospheric heat transport associated with the Hadley Cell is estimated to be ~ 0.4 PW into the southern hemisphere (Schneider *et al.* 2014), of which $>50\%$ is associated with the ISM (Heaviside and Czaja 2013). Although recent modeling results of the past ITCZ based on tropical SST gradients limits the global mean displacement to $< 1^\circ$ latitude (McGee *et al.* 2014), this result is heavily biased by the Pacific and Atlantic SSTs. Indeed, ISM rainfall is well correlated at present (Gadgil 2003) and in the past (Fleitmann *et al.* 2007) with the extent of northward migration of mean latitudinal position of the ITCZ.

The ITCZ always migrates towards the hemisphere that is warming more and its mean position is influenced by the inter-hemispheric temperature difference (Findlater 1969). This relationship has led to the monsoon being looked upon as responding to the Greenland climate (Deplazes *et al.* 2013; Hong *et al.* 2003; Marzinet *et al.* 2013; Sinha *et al.* 2005; Wang *et al.* 2001), but we argue here that the cross-equatorial heat transport associated with it, a consequence of meridional asymmetry, makes the ISM a viable candidate mechanism for forcing extratropical climate, in particular the deglacial cold reversals. Successful chronological synchronization of various polar climate records (Pedro *et al.* 2011) has enhanced confidence in relating radiocarbon dated oceanic climate proxy records with those of polar ice-core records.

Material and methods

A 4.2 m long sediment core (ABP32-GC01R) was raised from the Eastern Arabian Sea (EAS) at 15°29.49'N latitude and 72°43.64'E longitude from a water depth of 642 m (Fig. 1). The sediment core was sliced in to 2 cm subsections. The mixed planktonic foraminifera from six depth sections were subjected to radiocarbon dating at the Arizona University's AMS Facility, USA. In the upper 56 cm of the sediment core the abundance of planktonic foraminifera were not adequate for radiocarbon dating and the sections below 386 cm are not dated. The calculated sedimentation rates between two adjacent radiocarbon dated sections were used to develop the chronology for the sediment core (Table 1 and Fig. 2). The ages below 386 cm depth are extrapolated considering linear sedimentation rate as obtained for succeeding dated section 341-385 cm). Total time-span covered by the core is 18 to 4.5 ky BP. The reservoir age (622 y at 16.50°N and 73.93°E in the EAS: Southon et al., 2002) corrected ^{14}C ages were calibrated to calendar ages (reference year: 1950 AD) using Quickcal2007 Ver.1.5 (Danzeglocke et al. 2009) (Table 1).

The Mg/Ca measurement was carried out at 2 cm interval subsections (time resolution ~30-150 years), whereas, every second section was used for $\delta^{18}\text{O}$ measurements (time resolution ~60-300 years). The upper mixed layer dwelling planktonic foraminifera *G. sacculifer* (without terminal sac) that inhabits the upper mixed layer and is resistant to dissolution (Farmer et al. 2007) were handpicked from 250-355 μm coarse fractions, crushed between two glass plates. The fragments were homogenized with a fine brush and the visible clay lumps and oxide coated fragments were removed physically under microscope. Part of the aliquots were sent for $\delta^{18}\text{O}$ measurement at the Godwin Laboratory, Cambridge University, UK, and remaining part was subjected to cleaning protocol following Barker et al. (2003), that constitutes successive removal of clay, organic coating and secondary calcite-crust followed by dissolution in 0.075 M ultrapure HNO_3 .

The solutions were centrifuged at 14000 rpm for 10 minutes to eliminate any remaining sub-clay size particulates. The Mg/Ca (mmol/mol) was measured on an in-house Perkin-Elmer OPTIMA 7300 DV Simultaneous ICP-OES following intensity ratio calibration technique (DeVilliers et al. 2002). Further, to monitor any residual contamination by clays and oxides the Al, Fe, and Mn were also measured. A quality control solution with Mg/Ca = 4.46 mmol/mol was run at an interval of every five samples to monitor the effect of instrumental drift on measured Mg/Ca of samples and corrected following step-correction wherever required. The spectra of Al, Fe and Mn obtained for sample solutions appear mostly like the spectra for blank solution and their ratio with Ca rarely exceed 0.3 mmol/mol. The X-Y scatter plots of Al/Ca, Fe/Ca and Mn/Ca versus Mg/Ca exhibited no correlations. These data-quality observations suggest that the analyzed Mg/Ca is free from

contamination. The Mg/Ca (mmol/mol) measured in QC (n = 90) over the time of experiment is 4.46 ± 0.09 mmol/mol and for $\delta^{18}\text{O}$ the standard precision measurement is 0.1 ‰.

The Mg/Ca (mmol/mol) of *G. sacculifer* was translated in to SST utilizing a species specific calibration derived for the tropical Atlantic having modern annual average SST and surface salinity ($\sim 27.5^\circ\text{C}$ and 35.8 psu) (Dekens *et al.* 2002), which are closely comparable to the annual average SST and surface salinity at our core location ($\sim 28^\circ\text{C}$ and 35.6 psu: www.nodc.noaa.gov/WOA05). The $\delta^{18}\text{O}_{G.sacculifer}$ (Fig. 3) is a combined signal of temperature and $\delta^{18}\text{O}_{\text{WATER}}$. The former represents the SST since the *G.sacculifer* lives in well-mixed upper surface layer of the ocean and the latter represents a mixture of global ice-volume dependent whole ocean salinity and the local evaporation-precipitation forced local salinity. The global climate cooling (i.e., increased ice volume) results in increase of the $\delta^{18}\text{O}_{\text{WATER}}$ up to a maximum of 1 ‰ during the LGM (Shackleton 2000). Hence, the ice-volume corrected residual- $\delta^{18}\text{O}_{\text{WATER}}$, a proxy for local salinity provides a powerful tool to reconstruct the changes in local precipitation. The $\delta^{18}\text{O}_{\text{WATER}}$ is estimated from paleotemperature equation (Epstein *et al.* 1953) after correcting the $\delta^{18}\text{O}_{G.sacculifer}$ for global ice volume. This residual $\delta^{18}\text{O}_{\text{WATER}}$ represents the salinity in the EAS, in turn ITCZ-ISM associated precipitation. The surface salinity was estimated from $\delta^{18}\text{O}_{\text{WATER}}$ -Salinity relationship in the Arabian Sea (Dahl and Oppo 2006). The calculated 1 σ standard errors (Schmidt 1999) for each of the time-series are presented in Fig. 2.

We have adopted the temperature interpretations of $\delta^{18}\text{O}_{\text{ICE}}$ in Greenland (Monninet *al.* 2001; Stenni *et al.* 2001) and Temperature anomalies of Antarctic (Johnsen *et al.* 1992; Monninet *al.* 2001) for calculating relative changes in temperature. While discussing our results we keep in mind, 1) outside the upwelling cells of the Arabian Sea a significant SST cooling occurs due to strong summer monsoon wind-forcing in parts of the Arabian Sea (Murtugudde *et al.* 2007), and 2) the lead-lags in the climate seesaw of the order of ocean mixing time have been found to be statistically indistinguishable (Steig and Alley 2002) and hence are not considered to be of significance here. As our present sediment core location is not known for intense upwelling such as off Oman and off Somalia, the SST changes therefore are mostly associated with ISM wind forcing. The 1 σ error on SST ($\pm 0.96^\circ\text{C}$) and SS (± 0.6 psu) (Appendix) were calculated as the square-root of mean of the variance.

Results

We present centennial-resolution time-series of paired Mg/Ca SST and local- $\delta^{18}\text{O}_{\text{WATER}}$ (a proxy for local salinity controlled by Evaporation minus Precipitation (E – P or simply freshwater

flux) extracted from a sediment core of the EAS and compare the deglacial hydroclimate of the EAS and other tropical sites (Fig. 4) with the polar climate records in three relevant time slices: Bølling (~14.5 ka), ACR (~14.5–12.8 ka), and YD (~12.8–11.8 ka) (Table 1). The EAS precipitation is representative of the ISM because higher precipitation in this region reflects stronger winds blowing across the Arabian Sea and over the Indian subcontinent to the Bay of Bengal (Gadgil 2003), and also it includes freshwater input from several seasonal Western Ghat (Deccan) Mountain rivers.

Our data from the EAS show the two-step warming in the SST and decrease in $\delta^{18}\text{O}_{\text{WATER}}$ seen in the polar deglaciation pattern (Fig. 4). The SST increases from ~25.5°C to ~28 °C during pre-ACR, followed by a decrease of ~2°C during ACR, and remains cold (~26 °C) through the YD (Table 1). The $\delta^{18}\text{O}_{\text{WATER}}$, on the other hand, decreases from ~1.3 ‰ to 0.7 ‰ during pre-ACR, remains constant ~0.7 ‰ through the ACR, and increases to ~1.5 ‰ during the YD. This freshwater input pattern is also seen in marine records from the Eastern Equatorial Indian Ocean (EEIO) (Mohtadi *et al.* 2014) and southeastern Arabian Sea (Kessarkar *et al.* 2013), and in terrestrial precipitation records from northern China (Wang *et al.* 2001) and western Himalaya (Sinha *et al.* 2005): all show strong precipitation at the warmest Bølling, which nearly overlaps the commencement of ACR (Fig. 4). Likewise, the SST variation in the EAS is consistent with timings of SST variability in the EEIO (Mohtadi *et al.* 2014).

1. Discussion

Several tropical marine and terrestrial palaeo-records have suggested southward displacement of ITCZ during LGM (Clement and Peterson 2008; Schneider *et al.* 2014), resulting in significant reduction of ISM precipitation (Banakar *et al.* 2010; Deplazes *et al.* 2013). Considering the polar temperatures at the end of LGM (~18 ka) as reference temperatures for the respective hemispheres, the subsequent deglacial bipolar thermal contrasts are striking: at the Bølling and ACR the Greenland warmed by ~5 °C and 3 °C respectively more than the Antarctic and during the YD the Greenland warmed only ~1 °C as against ~7 °C warming in Antarctic as compared to their respective LGM temperatures (see Table 2 & Fig. 4). It is expected that a higher relative warmth in Greenland compared to Antarctica by 3–5 °C during the Bølling and ACR period (~14.5–12.8 ka) would have pulled the Indian Ocean ITCZ to the north from its LGM's southerly position, thereby intensifying the cross-equatorial winds and the Somali Jet (Findlater 1969) leading to enhanced ISM precipitation in particular and tropical precipitation in general. Our data and the other records suggest that intensified tropical precipitation that coincided with the warm Bølling of Greenland not only continued through the following Ållerød, but also were intense during the ACR of the Antarctica (Table 2 and Fig. 4).

From Table 2 it is evident that the north-south polar temperature gradients (between Greenland and Antarctica) at different climate events varied significantly [i.e, at LGM (18 ka) = 4°C, YD = 2°C, ACR = 7°C, Bølling = 9°C, and Holocene (modern) = 8 °C]. When compared to the present day temperature gradient of 8°C, that sets the modern location of the Indian Ocean mean ITCZ at ~5°N, the ITCZ at YD must have been most southward owing to significantly decreased bi-polar temperature gradient and most northward at the Bølling owing to significantly increased gradient. This means that the YD coincided with weakest ISM and the Bølling with strongest ISM, which are consistent with ISM intensity at different climatic events revealed by various sedimentary records (see Table 2). Thus, cross-equatorial heat transport associated with ITCZ-ISM may have played a definite role in dictating relative warmth in polar-regions.

When the ITCZ shifts north, it strengthens (weakens) the southern (northern) limb of the Hadley Cell because the ITCZ cannot shift poleward of the Himalayas, which act as a topographic barrier controlling the position of the northern hemisphere's subtropical jet stream (Ramaswamy 1956). Indeed, data from the Tropical Rainfall Measuring Mission (TRMM) show that intense precipitation occurs on the southern flanks of the Himalayas (Houze *et al.* 2007). When the southern limb of the Hadley Cell strengthens, more heat is exported to the southern hemisphere upper atmosphere, which is transmitted to the Antarctic by large-scale subtropical and polar eddies (Marshall and Plumb, 2008). Hence, a connection between polar temperatures and the ISM intensity is feasible.

The enhanced intensity of the ISM is associated with increased cross-equatorial heat transport in to the southern hemisphere via the strengthened Hadley Cell (Heaviside and Czaja, 2013), which in turn would transmit the heat to Antarctic through sub-tropical jets and polar eddies (see Figure 1) more effectively and rapidly than that by the returning warm surface arm of the AMOC. Hence, we hypothesize that a warming of the Greenland, could pull the ITCZ farther north over the Indian Ocean, which can reverse the Antarctic cooling via the intensified ISM. Therefore, following the Bølling the Antarctic recorded only ~3°C cooling during the ACR, whereas, corresponding Allerød in the Greenland recorded a cooling of ~5°C (Figure 4), due to loss of heat to southern hemisphere via the intense ISM. This interpretation is consistent with enhanced southern subtropical atmospheric circulation during the ACR (Stenni *et al.* 2001). Two lines of evidences can be provided in support of our hypothesis. The first line of evidence is an anti-correlation between the Antarctic sea-ice extent and the all India monsoon rainfall intensity on annual timescale in the modern time (1979-1999 dataset: Dugam and Kakade, 2004). That is, an increased ISM rainfall warms the Antarctic region leading to decreased sea-ice extent and vice-versa. The second line of evidence is that the last three

deglacial warmest events in Antarctic have been associated with synchronous weakening of the Asian Monsoons on millennial timescales (Chen et al., 2016). That is, long-term warming of the Antarctic forces the Asian Monsoons to weaken, apparently by pulling mean position of the ITCZ southward.

Our hypothesis implies that the excess thermal energy reaching the extratropics of the southern hemisphere during the ACR arrested the Antarctic cooling only to $\sim 3^\circ\text{C}$ (Parrenin et al. 2007; Jouzel et al. 1995) and terminated it at ~ 12.8 ka. The corresponding reduction of thermal energy reaching northern hemisphere extratropics would have forced the Greenland to cool further through the Ållerød resulting the YD, which is in antiphase with the ACR. With the onset of YD, the intense ITCZ-ISM precipitation, which was sustained through the ACR-Ållerød, would reach its nadir, as reflected in the decreased ISM over a vast tropical regime (Fig. 4). The accumulated thermal energy in the southern hemisphere throughout the ACR, evident in warming of the Southern Indian Ocean at that time (Stenni et al. 2001), might have rendered Antarctica to warm by $\sim 3^\circ\text{C}$ when the YD conditions were prevalent in the Greenland. Relatively more warmed Antarctic during the YD appears to have reduced the bi-polar temperature gradient to minimum (2°C : Table 2) that would force the mean ITCZ to migrate to its extreme southward position leading to significant weakening of the ISM. A significantly weakened ISM during the YD in turn might have reduced the cross-equatorial transport of northern hemisphere heat in to the southern hemisphere leading to rapid restoration of warming in Greenland to terminate the YD.

Conclusions

In summary, we hypothesize that the differentially cooled cold reversals in polar climates during the last deglaciation appear to have driven by meridional shifts in the ITCZ over the Indian Ocean and the associated changes in the ISM. It is unlikely that any single mechanism, whether CO_2 , AMOC, or tropical forcing via the ISM, will suffice to explain all the events seen in the palaeoclimate records. It is more likely that the global climate system consists of several cause-effect relationships, all interacting to effect the observed changes in climate. This hypothesis of tropical forcing of polar cold reversals, via the ISM, fills a niche in the jigsaw puzzle that constitutes the complex global climate system. The proposed tropical-atmospheric hypothesis driving the deglacial global climate if validated by simulation experiments has a potential to contribute to the development of predictive models of global climate under anthropogenic forcing.

Acknowledgments

This work is the part of the GEOSINKS Program funded by the CSIR. DS thanks MoES for funding through their CTCZ program. The sediment core was collected with the assistance of crew on board RV Boris Petrov chartered by the MoES for Cobalt-Crust Exploration program. SB thanks CSIR for her research fellowship. We thank Mike Hall and James Rolfe for oxygen isotope measurements at Godwin Laboratory, University of Cambridge, UK and DeMartino Mitzi of the Arizona University, USA for AMS-radiocarbon measurements. The constructive reviews by anonymous reviewers were of great help while revising the manuscript. *This is NIO contribution No.....*

References

- Banakar, V.K. *et al.* (2010) Climatology of the Eastern Arabian Sea during the last glacial cycle reconstructed from paired measurements of foraminiferal $\delta^{18}\text{O}$ and Mg/Ca. *Quat. Res.* **73**, 535-540.
- Barker, S. *et al.* (2009) Interhemispheric Atlantic seesaw response during the last deglaciation. *Nature* **457**, 1097-1102.
- Barker, S. *et al.* (2003) A study of cleaning procedures used for foraminiferal Mg/Capaleothermometry. *Geochem. Geophys. Geosyst.* **4**, 8407.
- Blunier, T. and Brook, E. J. (2001) Timing of millennial-scale climate change in Antarctica and Greenland during the Last Glacial Period. *Science* **291**, 109-112.
- Brown, E. T. *et al.* (2007) Abrupt change in tropical African climate linked to the bipolar seesaw over the past 55000 years. *Geophys. Res. Lett.* **34**, L20702.
- Calvo, E. *et al.* (2007) Antarctic deglacial pattern in a 30 kyr record of sea surface temperature offshore south Australia. *Geophys. Res. Lett.* **34**, L13707.
- Cane, M. A. (1998) A role for the tropical Pacific. *Science* **282**, 59-61.
- Chen, S. *et al.* (2016) Strong coupling of Asian monsoon and Antarctic climates on sub-orbital timescales. *Sci. Rep.* DOI: 10.1038/srep32995.
- Chiang, J. C. H. (2009) The tropics in paleoclimate. *Ann. Rev. Earth Planet Sci.* **37**, 263-297
- Clement, A. C. and Peterson, L. C. (2008) Mechanism of abrupt climate change of the last glacial period. *Rev. Geophys.* **46**, RG4002.
- Crowley, T. J. (1992) North Atlantic deep-water cools the southern hemisphere. *Paleoceanogr.* **7**, 489-497.
- Dahl, A.K. and Oppo, D.W. (2006) Sea surface temperature pattern reconstructions in the Arabian Sea. *Paleoceanogr.* **21**, PA1014, doi: 10.1029/2005PA001162.
- Danzeglocke, U., Joris, O. and Weninger, B. (2009) CalPal-2007^{ONLINE}. www.calpal-online.de.

- DePlazes, G. *et al.* (2013). Links between tropical rainfall and north Atlantic climate during the last glacial period. *Nature Geosci.* **6**, 213-217.
- Dekens, P. S. *et al.* (2002) Core-top calibration of Mg/Ca in tropical foraminifera: refining paleotemperature estimation. *Geochem. Geophys. Geosyst.* **3**, 1022-1036.
- DeVilliers, S. *et al.* (2002) An intensity ratio calibration method for accurate determination of Mg/Ca and Sr/Ca of marine carbonates by ICP-AES. *Geochem. Geophys. Geosyst.* **3**, 1001-1010.
- Dugam, K. K. and Kokade, S. B. (2004) Antarctic sea-ice and monsoon variability. *Indian J. Radio & Space Phys.* **33**, 306-309.
- Epstein, S. *et al.* (1953) Revised carbonate-water isotopic temperature scale. *Bull. Geol. Soc. Am.* **64**, 1315-1325.
- Farmer, E. C. *et al.* (2007) Corroborating ecological depth preferences of planktonic foraminifera in the tropical Atlantic with the stable isotope ratios of core-top specimen. *Paleoceanogr.* **22**, PA3205.
- Findlater, J. (1969) A major low level air current near the Indian Ocean during northern summer. *Quat. J. R. Meteor. Soc.* **95**, 362-380.
- Fleitmann, D. *et al.* (2007) Holocene ITCZ and Indian monsoon dynamics recorded in stalagmites from Oman and Yemen. *Quat. Sci. Rev.* **26**, 170-188.
- Gadgil, S. (2003) The Indian monsoon and its variability. *Ann. Rev. Earth Planet. Sci.* **31**, 429-467.
- Heaviside, C. and Czaja, A. (2013) Deconstructing the Hadley Cell heat transport. *Q. J. R. Meteorol. Soc.* **139**, 2181-2189.
- Hong, Y. T. (2003) Correlation between Indian Ocean summer monsoon and north Atlantic climate during the Holocene. *Earth Planet. Sci. Lett.* **211**, 371-380.
- Houze, Jr. R. A. *et al.* (2007) Monsoon convection in the Himalayan region as seen by the TRMM precipitation radar. *Quat. J. R. Meteorol. Soc.* **133**, 1389-1411.
- Johnsen, S. J. *et al.* (1992) Irregular glacial interstadials recorded in a new Greenland ice core. *Nature*, **359**, 311-313.
- Jones, P. D. (1990) Antarctic temperatures over the present century – a study of the early expedition record. *J. Clim.* **3**, 1193-1203.
- Jouzel, J. *et al.* (1995) The two step shape and timing of the last deglaciation in Antarctica. *Clim. Dyn.* **11**, 151-161.
- Karlsson, J. and Svensson, G. (2011) The simulation of Arctic clouds and their influence on the winter surface temperature in present-day climate in the CMIP3 multi-model dataset. *Clim. Dyn.* **36**, 623-635.
- Kesslerkar, P. M. *et al.* (2013) Variation in the Indian summer monsoon intensity during the Bølling-Ållerød and Holocene. *Paleoceanogr.* **28**, 413-425.

- Koutavas, A. *et al.* (2002) El-Nino like pattern in ice age tropical Pacific sea surface temperatures. *Science***297**,226-230.
- Marzin, C. *et al.* (2013) Glacial fluctuations of the Indian monsoon and their relationship with north Atlantic climate: new data and modeling experiments. *Clim. Past.* **9**, 2135-2151.
- McGee, D. *et al.* (2014) Changes in ITCZ location and cross-equatorial heat transport at the Last Glacial Maximum, Heinrich Stadial-1 and the mid-Holocene. *Earth Planet. Sci. Lett.* **390**, 69-79.
- Marshall, J. and Plumb, R. A. 2008. The general circulation of the atmosphere. (In: R. Dmowska, D. Hrtmann and H. T. Rossby (eds), Atmosphere, ocean, and climate dynamics – An introductory text. Internat. Geophys. Union, Ser. Monogr., 93, pp. 319.
- Mohtadi, M. *et al.* (2014) North Atlantic forcing of tropical Indian Ocean climate. *Nature***509**, 76-80.
- Monnin, E. *et al.* (2001) Atmospheric CO₂ concentration over the last glacial termination. *Science***291**, 112-114.
- Murtugudde, R. *et al.* (2007) Arabian Sea response to monsoon variation. *Paleoceanogr.* **22**, PA4217.
- Parrenin, F. *et al.* (2007) The EDC3 chronology for the EPICA Dome-C ice core. *Clim. Past.* **3**, 485-497.
- Pedro, J. B. *et al.* (2011) The last deglaciation: timing the bipolar seesaw. *Clim. Past.* **7**, 671-673.
- Philander, S. *et al.* (1996) Why the ITCZ is mostly north of the equator. *J. Clim.* **9**, 2958-2972.
- Ramaswamy, C. (1956) On the sub-tropical jet stream and its role in the development of large scale convection. *Tellus***8**, 26-59.
- Schmidt, G. A. (1999) Error analysis of palaeosalinity calculations. *Paleoceanogr.* **14**, 422-429.
- Schneider, T. *et al.* (2014) Migration and dynamics of the intertropical convergence zone. *Nature***513**, 45-53.
- Shackleton, N. J. (2000) The 100000 year ice-age cycle identified and found to lag temperature, carbon dioxide and orbital eccentricity. *Science***289**, 1897-1902.
- Shakun, J. D. (2012) *et al.*, Global warming preceded by increasing carbon-dioxide concentration during the deglaciation. *Nature***484**, 49-54.
- Sinha, A. *et al.* (2005) Variability of southwest Indian summer monsoon precipitation during the Bolling-Allerod. *Geol.* **33**, 813-816.
- Southon, J. *et al.* (2002) Marine reservoir correction for the Indian Ocean and southeast Asia. *Radiocarbon***44**, 167-180.
- Steig, E. J. and Alley, R. B. (2002) Phase relationship between Antarctic and Greenland climate records. *Annals Glaciol.* **35**, 451-456.

- Stenni, B., *et al.* (2001) An oceanic cold reversal during the last deglaciation. *Science*, **293**, 2074-2077.
- Svensson, A. *et al.* (2008) A 60000 y Greenland stratigraphic ice core chronology. *Clim. Past*, **4**, 47-57.
- Waliser, D.E. and Jiang, X. (2014) Tropical meteorology: Intertropical convergence zone. *Encycl. Atmos. Sci.*, Ed. **2**, Elsevier. doi: 10.1016/B978-0-12-382225-3.00417-5.
- Wang, Y. J. *et al.* (2001) A high resolution absolute-dated late Pleistocene monsoon records from Hulu caves, China. *Science* **294**, 2345-2348.
- Wunsch, C. (2006) Abrupt climate change: an alternative view. *Quat. Res.* **65**, 191-203.

Table 1. Details of radiocarbon ages with associated errors

Interval (cm)	Lab Ref. Number	¹⁴ C Age (years BP)	*Calendar Age (years BP)
58-60	AA94193	4665 ± 41	4528 ± 68
124-126	AA94194	9665 ± 52	10216 ± 25
200-202	AA94195	10481 ± 55	11280 ± 48
256-258	AA94196	11283 ± 59	12659 ± 67
340-342	AA94197	13055 ± 65	14683 ± 331
384-386	AA94198	14262 ± 72	16723 ± 264

* Based on the reservoir age corrected (622 y: Southon et al., 2002). Reference year is 1950 AD.

Table 2. Deglacial polar climate and corresponding tropical monsoon climate variability with respect to the LGM climate scenario

Record (see Fig. 3)	Bølling	ACR ^{\$}	YD	Ref.
*Greenland Temperature (a)	+11°C (–15°C)	+6°C (–20°C)	+1°C (–25°C)	1,2
Chinese rains: $\delta^{18}\text{O}_{\text{stalagmite}}$ (b)	Strong: ~ –0.5‰	Strong: ~ –6.5 ‰	Weak: ~ –6 ‰	3
ISM rains- EAS: $\delta^{18}\text{O}_{\text{seawater}}$ (c)	Strong: ~ 0.7 ‰	Strong: ~ 0.6 ‰	Weak: ~ 1.3 ‰	#
ITCZ rains- EEIO: $\delta^{18}\text{O}_{\text{seawater}}$ (d)	Strong: ~ 0.1‰	Strong: ~ 0.0 ‰	Weak: ~ 0.5 ‰	4
EAS SST (e)	2°C rise	---- 1.5°C colder pause	----	#
EEIO SST (f)	2°C rise	---- 0.5°C colder pause	----	4
Antarctic CO ₂ (g)	~50 ppmv rise	---- ~240 ppmv pause	----	5
*Antarctic temperature (h)	+6°C (–24°C)	+3°C (–27°C)	+7°C (–23°C)	2
N-S Temperature gradient	9°C	7°C	2°C	

*- Temperature changes in the polar regions with reference to their respective temperatures at ~18 ka (LGM). Values in parenthesis are the actual temperatures expected during different climate events. At present (Holocene), observed annual average temperature north of Arctic Circle is ~ –15°C (Karlsson and Svensson, 2011) and at Little America, western Ross Sea of Antarctica is ~ –23°C (Jones, 1990), i.e., a modern temperature gradient of ~8°C. Back-tracking the temperatures to the end of LGM, based on temperature changes recorded in ice-cores (Jouzelet *et al.* 1995), yield ~ –26°C for Greenland and ~ –30°C for Antarctica, i.e., a temperature gradient of ~4°C. These polar temperatures define the reference climate for 1) LGM to estimate past relative changes in respective polar temperatures, and 2) bipolar temperature set-up required to sustain the present position of the Indian Ocean ITCZ at ~5°N. Reduced temperature gradient at the LGM to ~6 °C as compared to modern 10 °C might have caused southward displacement of the ITCZ, probably close to the Equator. Lowest temperature gradient at the YD might have resulted in the collapse of summer monsoons in the northern hemisphere as a result of extreme southward shift of the ITCZ. The letters in parentheses in the first column refer to the panels in Fig. 3. # - Present study; 1- Jouzelet *et al.* (1995), Johnsen *et al.* (1992); 2- Parrenin *et al.* (2007); 3 – Wang *et al.* (2001); 4- Mohtadi *et al.* (2014); 5 – Monnin *et al.* (2001)]. \$ - The timing of ACR cold phase in Antarctica overlaps the timing of Ållerød cooling phase in Greenland.

FIGURE - 1

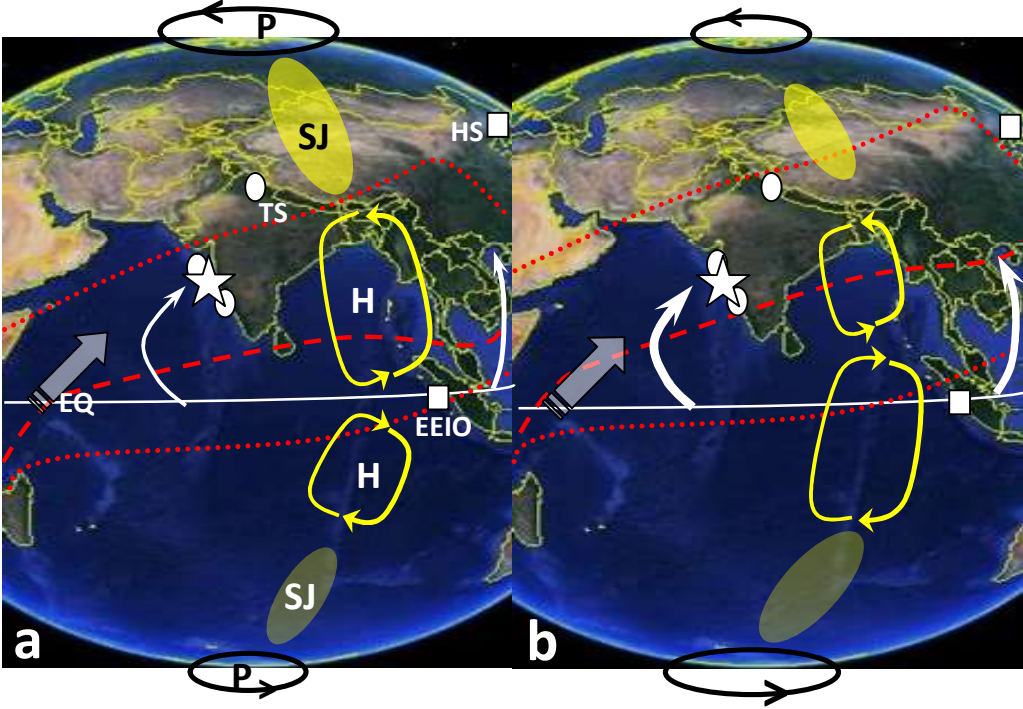


FIGURE 2

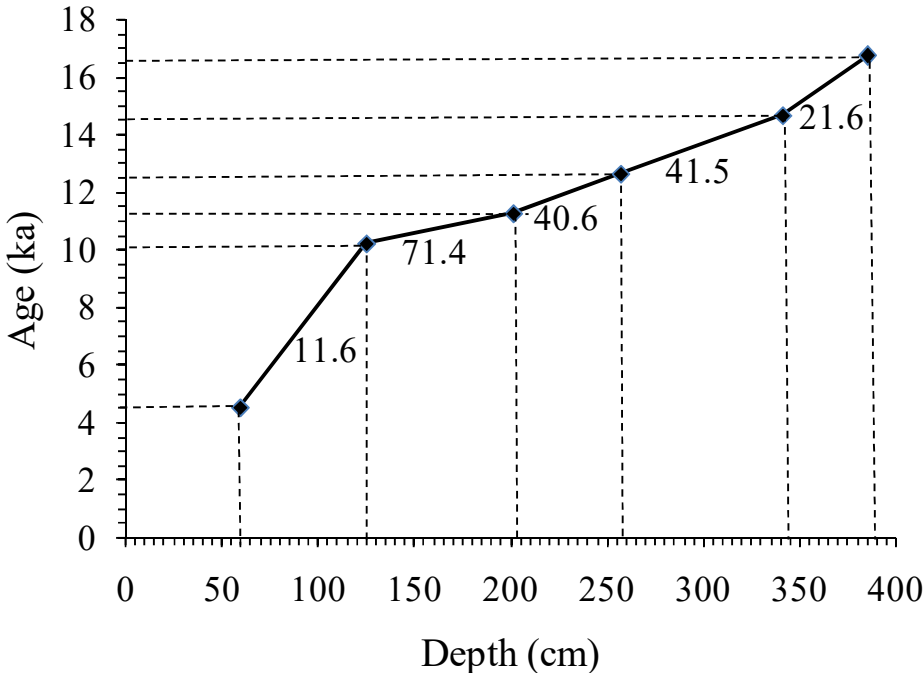


FIGURE -3

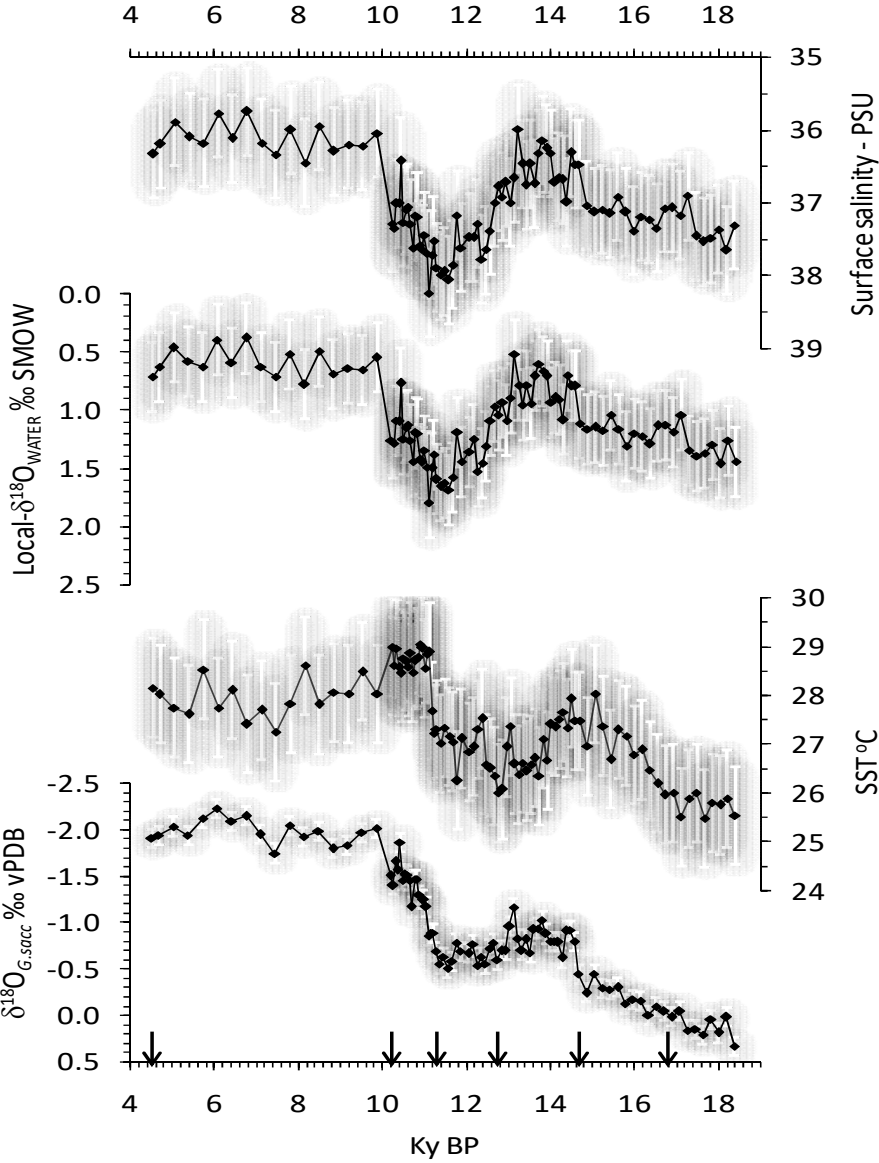


FIGURE - 4

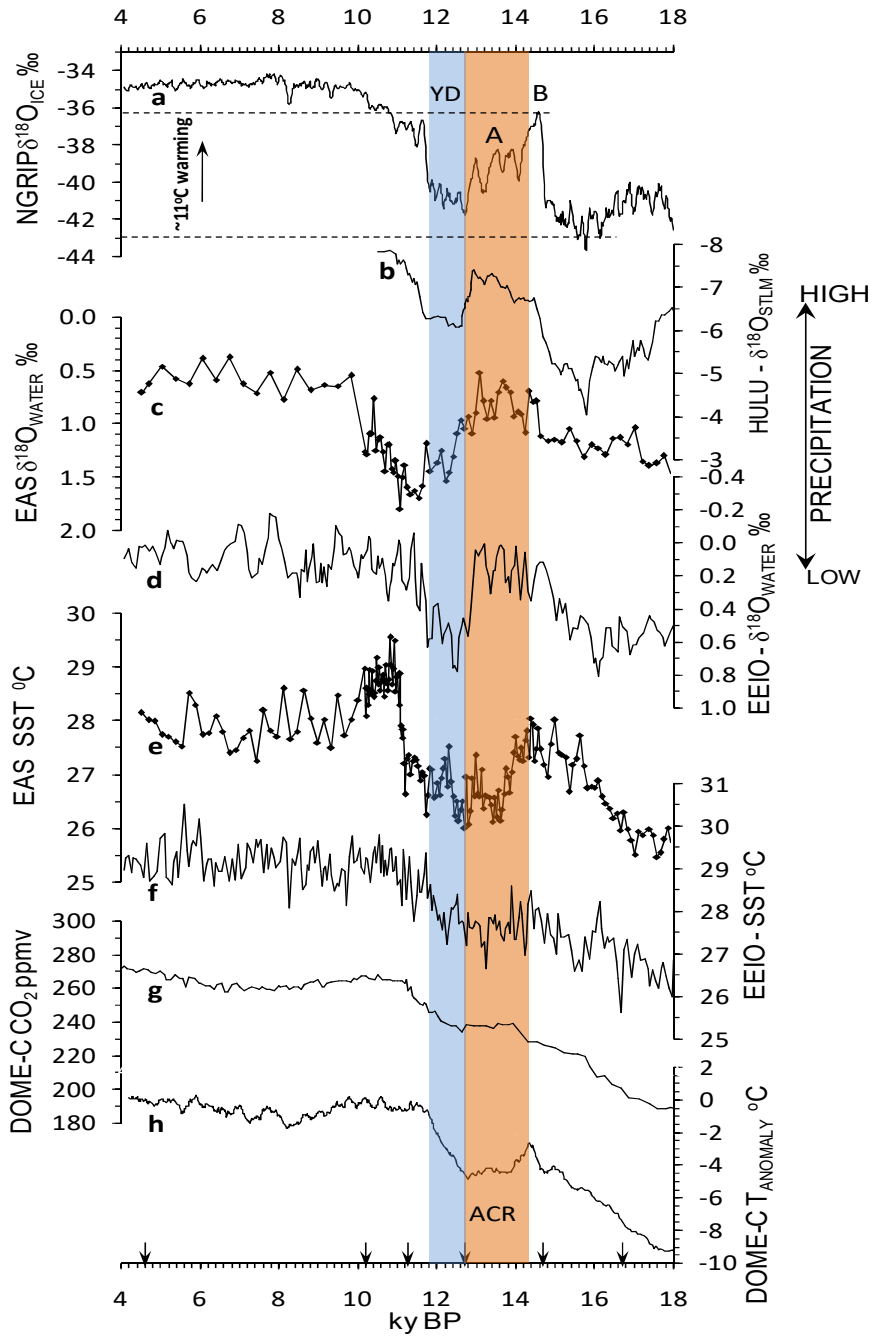


Figure Captions

Figure 1. Schematic drawing depicting present day atmospheric scenario (a) and likely scenario during the Bølling-ACR (b). Location of the present sediment core (ABP32-GC01R) from the EAS (white star) shown along with other tropical palaeomonsoon records presented in Figure 3 [white squares: HS – Hulu Cave stalagmite, Northern China (Wang *et al.* 2001), and EEIO – EasFtern Equatorial Indian Ocean sediment core SO189-39KL (Mohtadiet *al.* 2014) and those showing remarkably similar deglacial precipitation records but not shown in Fig. 4 (white circles), TS - Timta Cave stalagmite, western Himalaya (Sinhaet *al.* 2005), and Southern-EAS (Kessarkaret *al.* 2013)] The seasonal swing of ITCZ is shown with red dotted curved lines and its mean latitudinal position with broken red line (Gadgil 2003). In ‘b’ the mean position of the ITCZ and its seasonal swing are arbitrarily shifted by $\sim 5^\circ$ northwards from the present scenario. Atmospheric circulation (labeled curved arrows) responsible for interhemispheric heat distribution are labeled in panel ‘a’ [H = Tropical Hadley Cell – upward arrows indicate rising warm-flank of the cell and downward arrows are sinking-cold flank; SJ = Subtropical Jets-Large scale eddies; P = Polar eddies adopted from Marshall and Plumb (2008)]. Somali Jet, a major contributor of static moisture to the Indian Summer Monsoons (Heaviside and Czaja 2013) is shown with grey-shaded block-arrow and summer monsoon flow is shown with curved white arrows wherein the thickness of arrows indicate arbitrary relative strength during two climate scenarios, ‘a’ and ‘b’. EQ = Equator. The background map is adopted from www.google.com/earth (US Dept of State Geographer ©2016 Google) under their universal fair-use license.

Figure 2. Depth versus age model derived from five radiocarbon dated intervals (see Table 1). The calculated sedimentation rate (cm/ky) is shown for each sediment segment between two adjacent dated sections.

Figure 3. The time-series of $\delta^{18}\text{O}$ of *G.sacculifer*, Mg/Ca derived SST (Dekenset *al.* 2002), $\delta^{18}\text{O}_{\text{WATER}}$ derived from Epstein *et al.* (1953) palaeotemperature equation and surface salinity derived from $\delta^{18}\text{O}_{\text{WATER}}$ (Dahl and Oppo 2006) obtained from ABP32-GC01R. Capped vertical lines are 1σ error bars and grey-shaded background is the propagation of error through the dataset (See Appendix). Downward arrows are the radiocarbon dated sections.

Figure 4. Deglacial evolution of polar and monsoonal regimes from the last glacial maximum to the present the abscissa shows time in kiloyears before Present. Panels are arranged in order from north to south. (a) Greenland climate (Svenssonet *al.* 2008) (5-point moving average); (b) Chinese monsoon precipitation (Wang *et al.* 2001); (c) Eastern Arabian Sea precipitation (our data); (d) Eastern Equatorial Indian Ocean precipitation (Mohtadiet *al.* 2014) (3-point moving average); (e) Eastern Arabian Sea SST (our data); (f) Eastern Equatorial Indian Ocean SST (Mohtadiet *al.* 2014); (g) Antarctic DOME-C CO_2 record (Monninet *al.* 2001); (h) Antarctic DOME-C temperature anomaly (Parreninet *al.* 2007). Downward arrows indicate ages of radiocarbon dated sections of our sediment core from the Eastern Arabian Sea (c & e). ACR: Antarctic Cold Reversal - orange shaded bar; B: Bølling; A: Ållerød; YD: Younger Dryas - blue shaded bar. $\sim 11^\circ\text{C}$ warming at Bølling (a) is obtained from temperature conversion of $\delta^{18}\text{O}_{\text{ICE}}$ (Jouzelet *al.* 1995; Johnsenet *al.* 1992).

APPENDIX

Radiocarbon age (ka), $\delta^{18}\text{O}_{G.sacculifer}$ (‰ VPDB), Mg/Ca (mmol/mol), estimated SST (°C), estimated residual $-\delta^{18}\text{O}_{\text{SEAWATER}}$ (‰ VSMOW) and estimated surface salinity (psu) at the location of ABP32-GC01R sediment core.

Depth (cm)	Age (ka)	$\delta^{18}\text{O}_{G.sacculifer}$ (‰ VPDB)	Mg/Ca (mmol/mol)	SST (°C)	$-\delta^{18}\text{O}_{\text{SEAWATER}}$ (‰ VSMOW)	Salinity (PSU)
59	4.53	-1.91	4.718	28.2	0.71	36.3
61	4.70	-1.94	4.668	28.0	0.63	36.2
65	5.05	-2.04	4.550	27.7	0.46	35.9
69	5.39	-1.94	4.454	27.6	0.58	36.1
73	5.73	-2.13	4.819	28.5	0.63	36.2
77	6.08	-2.23	4.543	27.7	0.39	35.8
81	6.42	-2.1	4.221	26.8	0.59	36.1
85	6.77	-2.15	4.477	27.4	0.38	35.8
89	7.11	-1.95	4.600	27.7	0.63	36.2
93	7.46	-1.75	4.410	27.3	0.72	36.3
97	7.80	-2.05	4.630	27.8	0.52	36.0
101	8.15	-1.93	4.465	28.6	0.78	36.5
105	8.49	-1.99	4.614	27.8	0.49	36.0
109	8.84	-1.8	4.719	28.1	0.69	36.3
113	9.18	-1.84	4.705	28.0	0.64	36.2
117	9.53	-1.97	4.901	28.5	0.65	36.2
121	9.87	-2.02	4.706	28.0	0.55	36.0
125	10.22	-1.51	5.127	29.0	1.26	37.3
129	10.27	-1.4	4.960	28.6	1.28	37.3
133	10.33	-1.66	5.115	29.0	1.09	37.0
137	10.38	-1.57	4.940	28.6	1.10	37.0
141	10.44	-1.87	4.889	28.5	0.77	36.4
145	10.50	-1.45	5.024	28.8	1.25	37.3
149	10.55	-1.53	4.997	28.7	1.15	37.1
153	10.61	-1.52	4.942	28.6	1.13	37.1
157	10.66	-1.45	5.079	28.9	1.26	37.3
161	10.72	-1.17	4.892	28.5	1.44	37.6
165	10.78	-1.47	5.004	28.7	1.19	37.2
169	10.83	-1.47	5.032	28.8	1.20	37.2
173	10.89	-1.3	5.157	29.0	1.42	37.6
177	10.94	-1.25	5.122	29.0	1.45	37.6
181	11.00	-1.26	4.934	28.6	1.35	37.5
185	11.06	-1.17	5.066	28.8	1.49	37.7
189	11.11	-0.86	5.081	28.9	1.80	38.2
193	11.17	-0.89	4.564	27.7	1.50	37.7
197	11.22	-0.89	4.373	27.2	1.39	37.5
201	11.28	-0.69	4.410	27.3	1.60	37.9
205	11.38	-0.55	4.297	27.0	1.66	38.0
209	11.48	-0.63	4.421	27.3	1.62	37.9
213	11.58	-0.51	4.355	27.2	1.69	38.1

217	11.67	-0.58	4.312	27.1	1.58	37.9
221	11.77	-0.78	4.013	26.3	1.19	37.2
225	11.87	-0.69	4.336	27.1	1.44	37.6
233	12.07	-0.67	4.233	26.8	1.36	37.5
237	12.17	-0.77	4.270	26.9	1.25	37.5
241	12.27	-0.54	4.411	27.3	1.53	37.3
245	12.36	-0.63	4.497	27.5	1.46	37.8
249	12.46	-0.55	4.137	26.6	1.31	37.6
253	12.56	-0.72	4.108	26.5	1.09	37.4
257	12.66	-0.78	4.045	26.3	0.96	37.0
261	12.76	-0.6	3.925	26.0	1.04	36.8
265	12.85	-0.7	3.949	26.1	0.93	36.9
269	12.95	-0.7	4.269	26.9	1.09	36.7
273	13.04	-0.96	4.434	27.4	0.90	37.0
277	13.14	-1.16	4.138	26.6	0.52	36.7
281	13.24	-0.83	4.060	26.4	0.79	36.0
285	13.33	-0.7	4.142	26.6	0.95	36.5
289	13.43	-0.82	4.084	26.5	0.78	36.8
293	13.53	-0.68	4.134	26.6	0.94	36.5
297	13.62	-0.93	4.183	26.7	0.71	36.7
301	13.72	-0.94	4.048	26.4	0.60	36.3
305	13.82	-1.03	4.335	27.1	0.66	36.1
309	13.91	-0.88	4.167	26.7	0.71	36.3
313	14.01	-0.8	4.452	27.4	0.93	36.3
317	14.10	-0.8	4.428	27.4	0.89	36.7
321	14.20	-0.79	4.489	27.5	0.91	36.7
325	14.30	-0.62	4.550	27.7	1.08	36.7
329	14.39	-0.91	4.419	27.3	0.70	37.0
333	14.49	-0.92	4.666	27.9	0.79	36.3
337	14.59	-0.8	4.482	27.5	0.79	36.5
341	14.68	-0.45	4.480	27.5	1.11	36.5
345	14.87	-0.24	4.275	27.0	1.16	37.0
349	15.05	-0.45	4.704	28.0	1.15	37.1
353	15.24	-0.29	4.437	27.4	1.17	37.1
357	15.42	-0.28	4.171	26.7	1.04	37.1
361	15.61	-0.3	4.405	27.3	1.16	36.9
365	15.80	-0.13	4.357	27.2	1.31	37.1
369	15.98	-0.17	4.210	26.8	1.20	37.4
373	16.17	-0.16	4.247	26.9	1.22	37.2
377	16.35	0.00	4.092	26.5	1.29	37.2
381	16.54	-0.09	3.992	26.2	1.13	37.3
385	16.72	-0.04	3.911	26.0	1.13	37.1
389	16.91	0.02	3.921	26.0	1.19	37.1
393	17.09	-0.04	3.754	25.5	1.04	37.2
397	17.28	0.16	3.881	25.9	1.35	36.9
401	17.46	0.15	3.922	26.0	1.39	37.5

405	17.65	0.21	3.742	25.5	1.37	37.5
409	17.84	0.04	3.853	25.8	1.30	37.5
413	18.02	0.19	3.838	25.8	1.46	37.4
417	18.21	0.02	3.883	25.9	1.26	37.6
421	18.39	0.33	3.763	25.5	1.45	37.3
		MEAN	4.434	27.3	1.06	37.0
		1σ error		0.96	0.34	0.60